

An incorrect version of this article was published in *J. Mater. Res.*, Vol. 17, No. 9, September 2002. The correct version of the article appears here.

## Dielectric and piezoelectric properties of textured $\text{Sr}_{0.53}\text{Ba}_{0.47}\text{Nb}_2\text{O}_6$ ceramics prepared by templated grain growth

Cihangir Duran,<sup>a)</sup> Susan Trolier-McKinstry, and Gary L. Messing  
*Materials Science and Engineering Department, Materials Research Institute, Pennsylvania State University, University Park, Pennsylvania 16802*

(Received 11 November 2001; accepted 24 June 2002)

Fiber textured  $\text{Sr}_{0.53}\text{Ba}_{0.47}\text{Nb}_2\text{O}_6$  ceramics were reactively sintered to  $\geq 95\%$  of the theoretical density from a mixture of  $\text{SrNb}_2\text{O}_6$  and  $\text{BaNb}_2\text{O}_6$  powders. Texture in  $\langle 001 \rangle$  was obtained by templated grain growth on  $\langle 001 \rangle$ -oriented acicular  $\text{KSr}_2\text{Nb}_5\text{O}_{15}$  template particles. The most highly textured ceramics had a peak dielectric constant of 23,600 (at  $T_c = 128^\circ\text{C}$ ), a remanent polarization ( $P_r$ ) of  $20.3 \mu\text{C}/\text{cm}^2$ , a saturation polarization ( $P_{\text{sat}}$ ) of  $24 \mu\text{C}/\text{cm}^2$  (69–96% of single crystal), and a piezoelectric charge coefficient ( $d_{33}$ ) of  $84 \text{ pC}/\text{N}$  (76–93% of single crystal). A model, correlating polarization with grain orientation, predicts that  $P_r$  increases sharply when a percolating grain network forms to transfer charge between elongated grains.

### I. INTRODUCTION

Electroceramics are used in a variety of applications such as sensors, actuators, capacitors, and varistors. In these applications, the ceramic microstructure often consists of equiaxed, randomly oriented grains. Ferroelectric transducers require poling to obtain useful piezoelectric properties. Poling is difficult for some ferroelectric ceramics because the symmetry-related orientations available for the spontaneous polarization are limited.<sup>1</sup>

Nagata *et al.*<sup>2</sup> achieved anisotropic properties by hot pressing SBN ceramics ( $x = 0.30\text{--}0.65$ ), but their polarization values were well below the single-crystal values. In an earlier paper, we reported enhanced electrical properties in highly textured  $\text{Sr}_{0.53}\text{Ba}_{0.47}\text{Nb}_2\text{O}_6$  (SBN53) ceramics fabricated by templated grain growth (TGG).<sup>3</sup> Acicular  $\text{KSr}_2\text{Nb}_5\text{O}_{15}$  (KSN) particles (5 to 15.4 wt%) and  $\text{V}_2\text{O}_5$  (0.8 mol%) were used as template and liquid former, respectively. It was found that texture development started at  $T < 1000^\circ\text{C}$  due to melting of  $\text{V}_2\text{O}_5$  at  $690^\circ\text{C}$ . Highly grain-oriented ceramics (texture fraction,  $f$ , approximately 0.93) had 60–84% of single-crystal saturation polarization and 80–98% of single-crystal strain coefficient ( $d_{33}$ ) in the polar ( $c$ ) direction. However, the peak dielectric properties were found to be much lower than the single-crystal values due to the presence of  $\text{V}_2\text{O}_5$ -based nonferroelectric phase(s) on the grain

boundaries. In addition, small template particles (especially  $< 5 \mu\text{m}$  in length) and anisotropic grain growth in the matrix were found to broaden the texture distribution in the polar axis, particularly at low template loadings. In this paper, we report a reactive templated grain growth process to obtain textured SBN53 in undoped and  $\text{Nb}_2\text{O}_5$ -rich matrices to avoid the deleterious effects of  $\text{V}_2\text{O}_5$  on dielectric properties. The electrical properties of textured SBN53 are compared to those of random samples, textured samples prepared with  $\text{V}_2\text{O}_5$ , and single crystals. A method is proposed to model the polarization behavior as a function of texture fraction and the degree of orientation distribution.

### II. EXPERIMENTAL

$\text{SrNb}_2\text{O}_6$  (SN) and  $\text{BaNb}_2\text{O}_6$  (BN) powders were used to prepare SBN53 ceramics by reactive sintering. Acicular KSN templates were used to texture SBN53 by TGG. Templates of  $1\text{--}3 \mu\text{m}$  in diameter and  $10\text{--}20 \mu\text{m}$  in length were physically separated by differential settling in water, to narrow the texture distribution. A detailed study of template particle and matrix powder synthesis (together with reactive versus conventional sintering) is given elsewhere.<sup>3,4</sup> The fiber axis is  $[001]$  (or  $c$  direction), which corresponds to the spontaneous polarization and fast crystal growth direction of SBN.

Table I summarizes the sample designation, KSN concentration, initial amounts of additives, and excess BN in the SBN53 samples. Because the composition of

<sup>a)</sup>Now with the Department of Materials Science and Engineering, Gebze Institute of Technology, Gebze, Turkey.

TABLE I. Sample designation, KSN content, and additive contribution in SBN53 ceramics.

Sample designation <sup>a</sup>	KSN content (wt%)	Additive contribution (wt%)		Excess BN (wt%)
		K <sub>2</sub> O	Nb <sub>2</sub> O <sub>5</sub>	
T5	5	0.26	0.72	4.05
T9	9.1	0.47	1.32	7.41
T12	12	0.62	1.74	9.71
T15	15.4	0.79	2.23	12.45
T5-9	5	0.47	1.32	4.05
T5-15	5	0.79	2.23	4.05

<sup>a</sup>T refers to textured samples.

template particles is different from that of the matrix powder, extra BN powder was added to compensate for the strontium and niobium introduced by the KSN templates. However, the potassium and some of the excess niobium from the KSN could not be compensated in the final composition. Therefore, the concentration of K<sub>2</sub>O and Nb<sub>2</sub>O<sub>5</sub> increases with increasing KSN concentration. For the T5-9 and T5-15 samples, only 5 wt% KSN templates were used. However, their compositions were adjusted to T9 and T15, respectively, by adding K<sub>2</sub>O (J.T. Baker, Philipsburg, NJ) and Nb<sub>2</sub>O<sub>5</sub> (H.C. Starck, Newton, MA). For comparison, random samples (denoted by R) were also prepared by tape casting, using KSN powder rather than acicular particles. Procedures to obtain oriented template particles in a mixture of SN and BN and to prepare samples for microstructure analysis were described earlier.<sup>3</sup>

After binder burnout, samples were heated at 7 °C/min to 1200–1450 °C and held for 1 min to 12 h. Sections were cut parallel (denoted by “//”) and perpendicular (denoted by “⊥”) to the casting direction from the textured samples. In other words, the symbols // and ⊥ stand for *a*–*b* oriented (non-polar) and *c*-oriented (polar) samples, respectively.

Crystallographic texture was characterized using x-ray diffractometry (XRD) on the ⊥-cut samples and the texture fraction, *f*, was calculated, using the Lotgering factor,

$$f = (P - P^{\circ}) / (1 - P^{\circ}) \quad (1)$$

where *P* and *P*<sup>°</sup> are  $[I_{(001)} + I_{(002)}] / \sum I_{(hkl)}$  in the textured and random cases, respectively. Scanning electron microscopy (SEM) micrographs of // -cut samples were used to characterize the morphological texture. Crystallographic orientation distribution was obtained from corrected rocking-curve (or ω-scan) measurements,<sup>5,6</sup> using the (002) SBN53 peak. The orientation distribution was calculated by fitting corrected rocking curves to the March–Dollase equation:<sup>7,8</sup>

$$Q(f, r, \alpha) = f(r^2 \cos^2 \alpha + r^{-1} \sin^2 \alpha)^{-3/2} + (1 - f) \quad (2)$$

where *f* is the texture fraction, *r* is the degree of orientation parameter, and α is the angle from the texture direction (e.g., [001]). The *r* is closely related to the

width of the orientation distribution of the anisotropic grains and ranges from *r* = 1 for random to *r* = 0 for perfectly textured materials.

The dielectric constants of normal ferroelectric ceramics can be expressed by the Curie–Weiss law above *T*<sub>c</sub> (or *T*<sub>max</sub>). However, the broad dielectric spectra of the relaxor ferroelectrics more appropriately follow a quadratic law.<sup>9</sup> To quantify the phase transition modes for the intermediate type ferroelectrics (e.g., neither normal nor relaxor), a power law combining the Curie–Weiss and the quadratic laws was proposed by Uchino and Nomura<sup>10</sup> and is given as

$$1/K = (1/K_{\max}) + [(T - T_{\max})^{\gamma}] / C \quad (3)$$

where *K* is the dielectric constant at *T*, *K*<sub>max</sub> is the dielectric constant at *T*<sub>max</sub>, γ is a diffuseness coefficient, and *C* is the Curie–Weiss constant. Equation (3) describes a normal ferroelectric when γ = 1 (the Curie–Weiss law) and a relaxor ferroelectric when γ = 2 (the quadratic law).<sup>11</sup>

Polarization–electric field (*P*–*E*) hysteresis data were measured at 10 Hz, using a modified Sawyer–Tower circuit. *P*–*E* data were recorded in two different ways; for the first, the maximum voltage was increased sequentially (e.g., 10, 20, 30 kV/cm) (type A), and for the second one, the sample was depoled by annealing at 500 °C for 1 h before each measurement (type B).

The fatigue behavior of the samples was also measured as a function of cycling using the same *P*–*E* circuit at 50 kV/cm, 10 Hz, and 25 °C. Poling was performed by

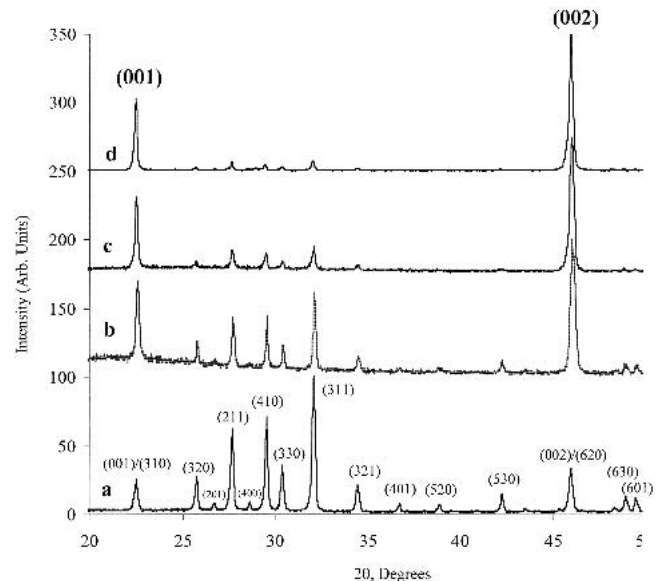


FIG. 1. XRD patterns of the T9⊥ samples after sintering for 4 h at (b) 1200 °C, (c) 1300 °C, and (d) 1400 °C. Curve “a” is for the random (R9) sample (heated at 1250 °C for 5 h) and given as an untextured reference pattern. Major SBN53 peaks (JCPDS No. 39-265) are marked.

applying 10 kV/cm at approximately 10–15 °C above  $T_c$  for 15 min and then cooling to room temperature while maintaining the field. Procedures to measure electrical properties were described earlier.<sup>3</sup>

### III. RESULTS

#### A. Densification and texture development

The relative theoretical density (TD) was based on the density of an SBN52 single crystal (5.33 g/cc),<sup>12</sup> which is close to the composition of interest. The samples reached  $\geq 95\%$  TD after sintering at temperatures  $\geq 1300$  °C for 4 h, and then densification leveled off regardless of the sintering temperature (for 4 h) and template content. For sintering at 1400 °C, the densities were nearly the same (approximately 96–98% TD) in samples heat-treated between 1 min and 12 h.

XRD patterns of the T9 $\perp$  samples as a function of sintering temperature as well as a reference pattern of random SBN53 (R9) sintered at 1250 °C for 5 h are given in Fig. 1. For the T9 samples, the  $\{00l\}$  peaks dominate the diffraction pattern as the sintering temperature increases. In addition, all samples transformed to the tetragonal tungsten bronze (TTB) structure by  $T = 1200$  °C. Figure 2 shows that morphological texture development increases with sintering temperature and/or time in the T9// samples. At 1200 °C, the matrix is still very porous and there is no overgrowth on the KSN templates. During the later stage of densification, the porosity starts to concentrate near template particles [Figs. 2(b) and (c)].

Figure 3 compares the effect of template concentration on texture development in the samples sintered at 1400 °C for 12 h. For the T5-T15 samples [Figs. 3(a)–(d)],

a template content of 5 wt% is insufficient for full texture development. Porosity in the samples increases with the template content. In addition, elongated grains are larger in dimension with decreasing template content except for the T5-15// sample. The average length and thickness of the grains in Fig. 3, calculated by the stereological method,<sup>13</sup> is  $36 \times 6 \mu\text{m}^2$  for T5-15,  $24 \times 4 \mu\text{m}^2$  for T5,  $17 \times 3 \mu\text{m}^2$  for T9, and  $14 \times 3 \mu\text{m}^2$  for T15 samples.

Crystallographic texture analysis was performed on the  $\perp$ -cut samples, using the Lotgering factor (Fig. 4). The texture fraction ( $f$ ) increases with increasing sintering temperature for all samples. Moreover, holding the samples at 1400 °C for 12 h resulted in enhancement in  $f$ . For example, the T5-15 samples attained  $f = 0.98$  compared to 0.61 for the T5 samples.

Orientation distribution curves for the samples sintered at 1400 °C for 12 h were obtained by fitting the corrected rocking curve data to Eq. (2), and then the  $r$  values were determined. The  $r$  values were found to decrease with decreasing template content; that is,  $r = 0.40$  for T15, 0.34 for T12, 0.32 for T9, and 0.29 for T5 and T5-15. Increase in the  $r$  parameter corresponds to a broadening of the orientation distribution in the  $c$  direction (i.e.,  $[001]$ ).

#### B. Dielectric properties

Figure 5 shows the orientation and temperature dependence of the dielectric properties at different frequencies for the T9 samples sintered at 1400 °C from 1 min to 12 h (samples are  $\geq 96.5\%$  dense). Figure 5(a) shows that the peak dielectric constant ( $K_{\text{max}}$ ) strongly improves in the  $c$  direction with sintering time. Dielectric spectra indicate relaxor behavior with a gradually

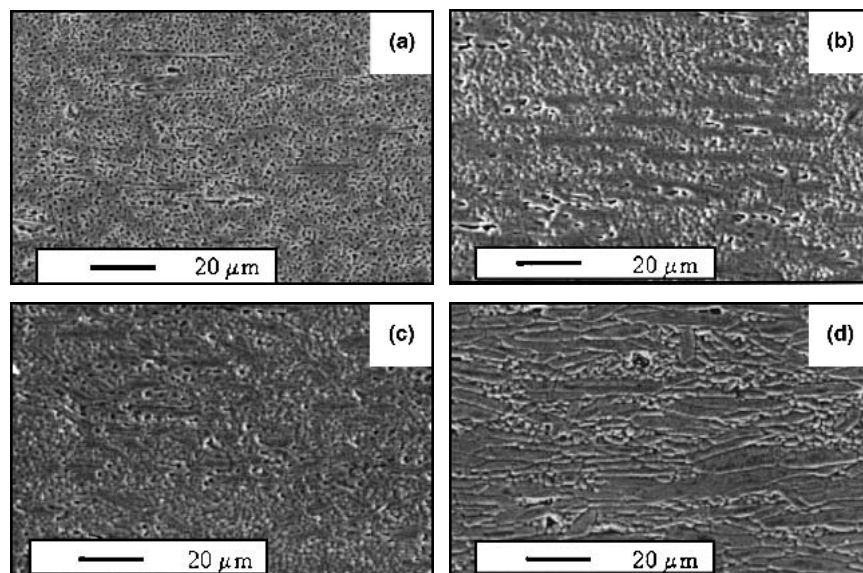


FIG. 2. Texture development in the T9// samples as a function of sintering conditions: (a) 1200 °C for 4 h; (b) 1300 °C for 4 h; (c) 1400 °C for 1 min; (d) 1400 °C for 4 h.

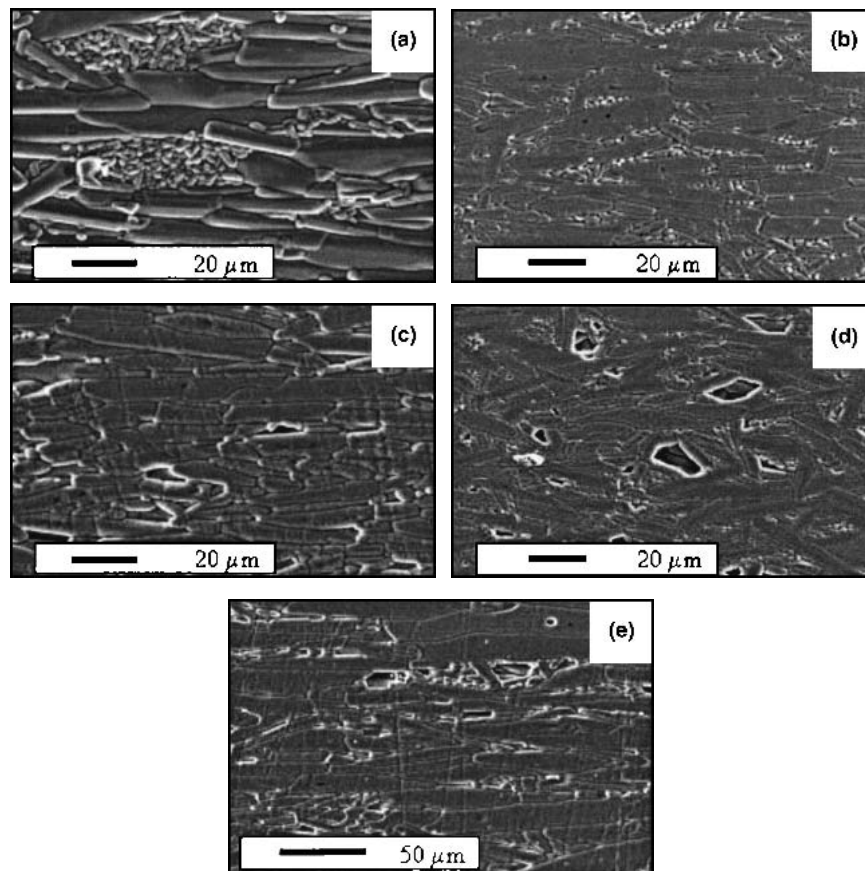


FIG. 3. Texture development as a function of template concentration after sintering at 1400 °C for 12 h: (a) T5//; (b) T9//; (c) T12//; (d) T15//; (e) T5-15//.

decreasing  $K_{\max}$  with frequency. In addition, the breadth of the phase transformation diminishes with sintering time. The frequency dependence of  $T_{\max}$  is more pronounced for the samples sintered for 1 min. Room-temperature dielectric constant ( $K_{\text{RT}}$ ) and  $K_{\max}$  are much lower in the nonpolar  $a$ - $b$  plane, shown as an inset in Fig. 5(a), and decrease with increasing sintering time. In addition, the frequency dispersion of the dielectric spectra diminishes with sintering time. The anisotropy in the dielectric properties is consistent with data on SBN single crystals. The two orientations also show different dielectric loss behaviors such that the loss is lower in the  $a$ - $b$  plane than the  $c$  direction. Unlike the  $a$ - $b$  plane, loss increases with sintering time in the  $c$  direction [Fig. 5(b)].

$K_{\max}$  in the  $c$  direction was found to increase with increasing initial template content and  $f$ . A maximum  $K_{\max}$  of 23,600 at  $f = 0.93$  was measured in the T9 $\perp$  samples.  $K_{\max}$  values of 1525 and 860 in the random (R9) and T9// were obtained, respectively. Although the T5-15 samples reached the highest texture fraction ( $f = 0.98$ ), they showed relatively lower  $K_{\max}$  (of 17,000).

The diffuseness coefficient ( $\gamma$ ) and degree of diffuseness ( $C/K_{\max}$ ) were calculated using Eq. (3). Figure 6

shows an analysis of  $(K_{\max}/K)$  versus  $(T - T_{\max})^\gamma$  at 100 kHz for the T9 $\perp$  samples sintered at various sintering conditions. Each line has a correlation coefficient ( $R^2$ )  $\geq 0.99$  to a linear fit. The inset shows  $f$ ,  $\gamma$ , and  $C/K_{\max}$  (in °C) as a function of sintering conditions. Samples sintered at 1400 °C for 1 min and 12 h have the lowest and highest  $K_{\max}$  values (5600 versus 23,600) and corresponding  $f$  values (0.6 versus 0.93), respectively.  $\gamma$  and  $C/K_{\max}$  decrease with increasing  $f$ .

### C. Switching and piezoelectric properties

When hysteresis ( $P$ - $E$ ) loops were recorded using progressively higher applied fields on highly textured T9 $\perp$  and T15 $\perp$  samples (type A), it was found that extremely rapid fatigue was observed [see Fig. 7(a)]. As a result, the remanent polarization ( $P_r$ ) decreased and coercive field ( $E_c$ ) increased on successive measurements. The decrease in switchable polarization with increasing measurement field could be avoided by heating the sample above  $T_c$  between measurements [type B in Fig. 7(b)]. In this case,  $P_r$  increases with the applied field. Highly textured T5-15 $\perp$  samples, however, did not show strong

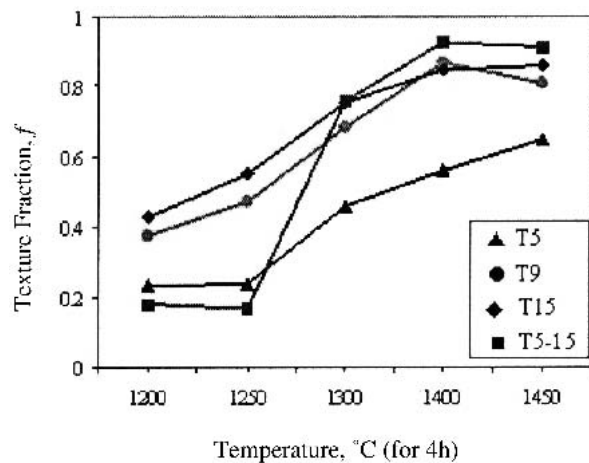


FIG. 4. Texture fraction ( $f$ ), calculated using the Lotgering factor, as a function of sintering temperature.

fatigue dependence and reached the highest  $P_r$  values [e.g.,  $P_r = 20.3 \mu\text{C}/\text{cm}^2$  at 50 kV/cm in Fig. 7(b)]. In the  $a$ - $b$  plane,  $P_r$  decreased with increasing texture fraction, and there was no evidence for fatigue.

Comparison of the  $P$ - $E$  loops as a function of crystallographic orientation and type of measurement is given in Fig. 8 for the T5-15 samples sintered at 1400 °C for 12 h. The random sample (R15) was sintered at 1350 °C for only 4 h to prevent abnormal grain growth that decreases  $P_r$  and increases  $E_c$ . The textured samples show strong anisotropy.

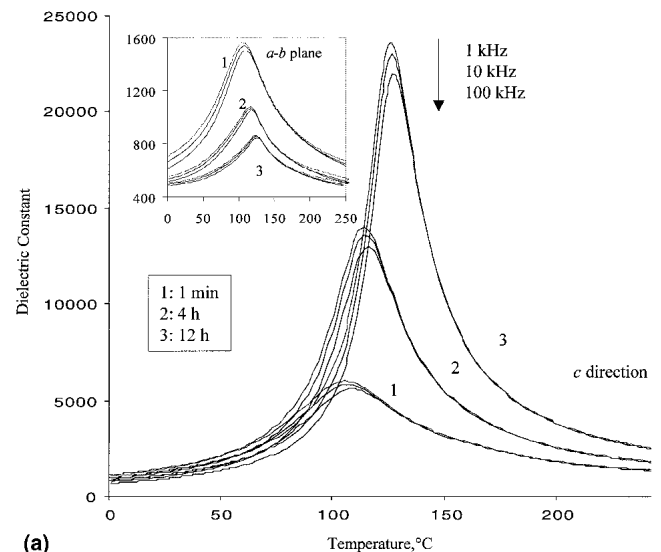
The remanent polarization was modeled on the basis of the processing parameters (i.e.,  $f$  and  $r$ ). SBN has a spontaneous polarization only in the  $c$  direction; that is,  $P_1 = P_2 = 0$  and  $P_3 \neq 0$ . Therefore, for misoriented grains, the polarization distribution can be expressed as  $P_3 \cos \alpha$ , where  $\alpha$  is the angle from the texture axis.

The orientation distribution in the  $c$  direction can be calculated using Eq. (2). The volume of material oriented at an angle  $\alpha$  changes as  $\sin \alpha$ .<sup>5</sup> Therefore, Eq. (2) can be multiplied by the sine function to determine the fraction of material as a function of  $\alpha$  (i.e., normalization of the March-Dollase function).

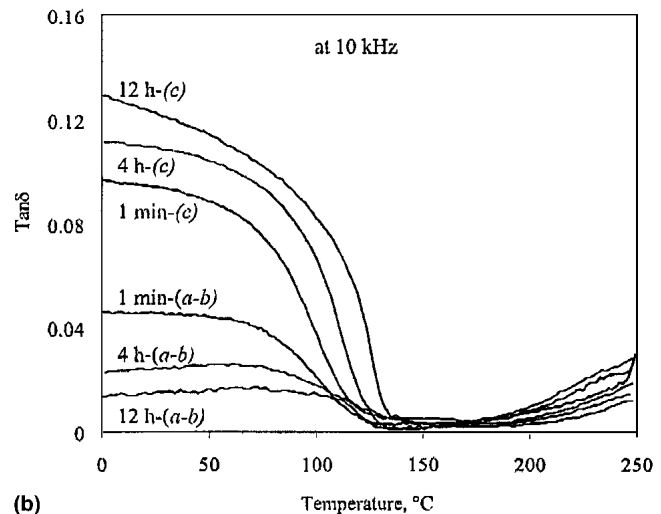
The polarization at any angle, therefore, can be found by multiplying the polarization distribution function with the normalized March-Dollase function,

$$P(r,f) = \int_0^{\pi/2} P_3 \cos \alpha [Q(f,r,\alpha) \sin \alpha] d \alpha \quad (4)$$

This equation calculates the maximum expected polarization as a function of experimentally determined  $r$  and  $f$  values. Measured  $P_r$  data were fit to this model, using  $f$  and  $r$  values for each composition. Calculated data from this modeling and measured  $P_r$  are given in Fig. 9. Calculated data yield the maximum polarization that can ideally be obtained for a given set of  $f$  and  $r$  (like



(a)



(b)

FIG. 5. Dielectric (a) constant and (b) loss as a function of sintering time and crystallographic (polar  $c$  and nonpolar  $a$  or  $b$ ) direction for the T9 samples. Samples were sintered at 1400 °C. The inset in (a) gives the data for measurements in the  $a$ - $b$  plane.

single crystals cut at certain angles and assembled together). It is clear that  $P_r$  remains constant until  $f \approx 0.5$  and then increases sharply.

## IV. DISCUSSION

### A. Densification and texture development

Densification increases with sintering temperature and levels off after sintering at temperatures  $\geq 1300$  °C for 4 h for all samples. Densification below 1300 °C was slowed due to SBN53 phase formation from the SN and BN mixture and compositional homogenization of cations in the TTB structure. The effect of  $\text{K}_2\text{O}$  and  $\text{Nb}_2\text{O}_5$  on densification and phase formation of SBN53 ceramics during reactive sintering is discussed in detail elsewhere.<sup>14</sup>

The final solid solution (e.g., SBN53) between the KSN and SBN starts at the template–matrix interface. This process is accelerated by a liquid phase. Lee *et al.*<sup>15,16</sup> found that  $\text{Nb}_2\text{O}_5$ -excess grain boundaries

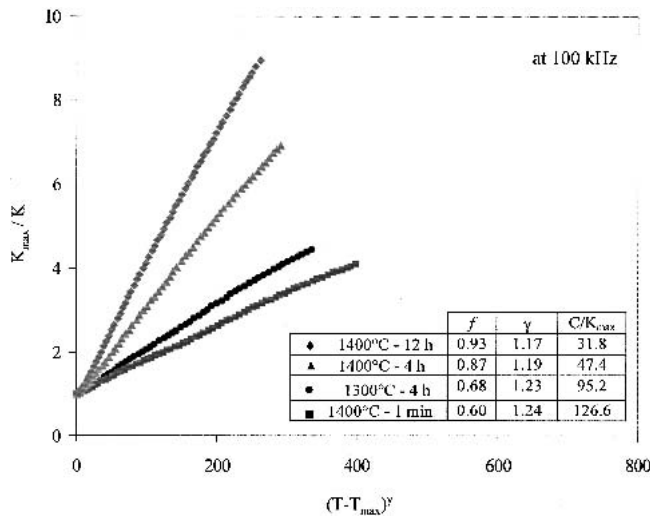


FIG. 6. Plot of  $K_{\max}/K$  versus  $(T - T_{\max})^\gamma$ , with calculated values of degree of diffuseness ( $C/K_{\max}$  in °C), as a function of sintering conditions for the T9± samples.  $f$  and  $\gamma$  stand for the texture fraction and diffuseness coefficient, respectively.

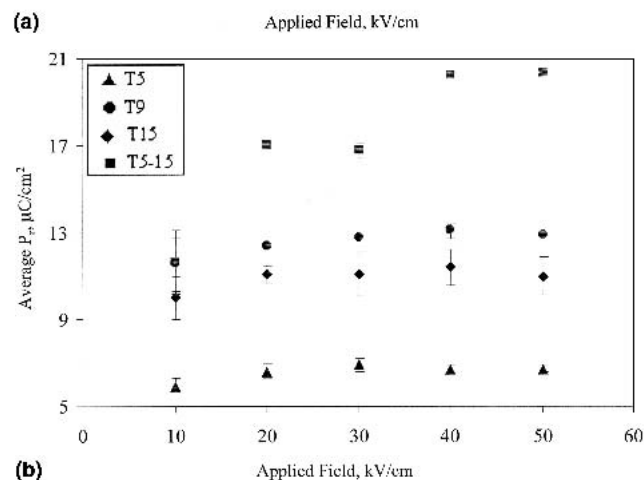
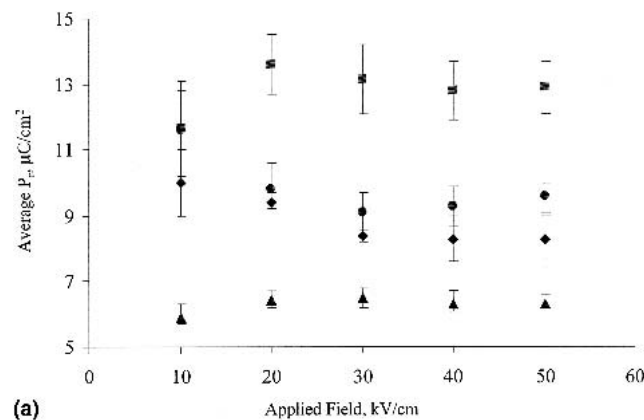


FIG. 7. Change of average remanent polarization ( $P_r$ ) as a function of initial template content in the  $c$  direction: (a) type A; (b) type B. Samples were sintered at 1400 °C for 12 h.

cause liquid formation at  $T \geq 1260$  °C, and the temperature at which the liquid phase forms decreases with more excess  $\text{Nb}_2\text{O}_5$ .<sup>17</sup> Therefore, liquid may form due to the presence of excess  $\text{Nb}_2\text{O}_5$  contributed from the KSN templates. The T5-9 and T5-15 samples, however, also have a liquid phase in the matrix due to the presence of  $\text{Nb}_2\text{O}_5$ , which makes the cation distribution more uniform in the matrix, compared to T5-T15 samples. Upon template growth, local homogenization (e.g., diffusion of  $\text{K}^+$ ,  $\text{Sr}^{2+}$ ,  $\text{Nb}^{5+}$ , and  $\text{Ba}^{2+}$  ions) can start inside the grown region with increasing sintering temperature and/or time.

Figure 4 indicates that  $f$  increases sharply for each set after 1300 °C, which indicates that densification of the matrix is required for template particles to grow.

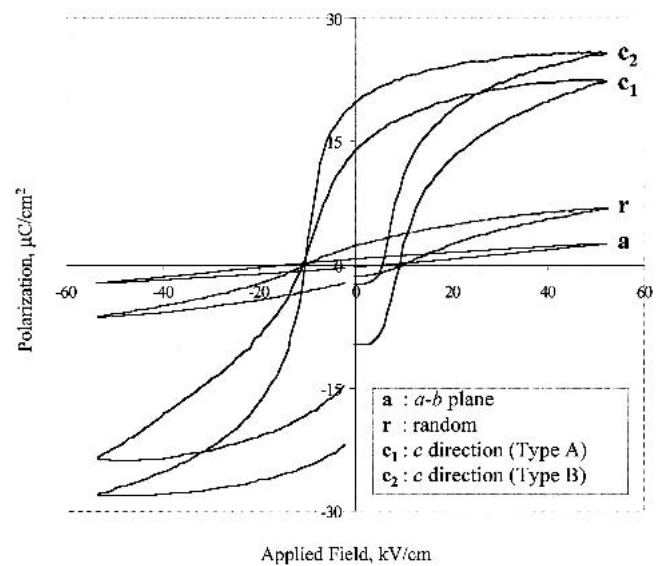


FIG. 8.  $P$ - $E$  hysteresis loops of the T5-15 samples sintered at 1400 °C for 12 h and random sample (R15) sintered at 1350 °C for 4 h.

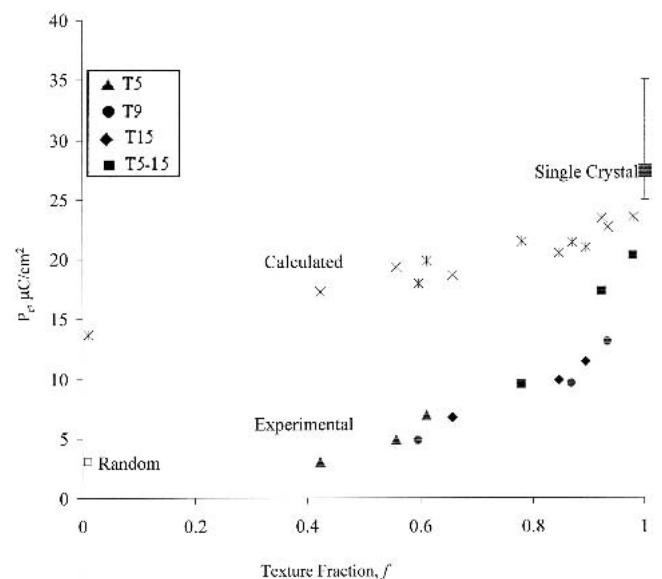


FIG. 9. Change of average  $P_r$  (type B) as a function of initial template content and  $f$ . Samples are  $\geq 95\%$  dense.

However the observed crystallographic orientation in [001] (“curve b” in Fig. 1) without significant template growth [Fig. 2(a)] suggests that texturing is mainly due to initially oriented KSN template particles at lower densification. Increase in  $f$  with sintering conditions (Fig. 4) results from the growth of templates in the matrix. An initial template concentration around 9 wt% is adequate to produce a highly textured microstructure ( $f = 0.93$ ) with a narrow distribution of anisotropic grains ( $r = 0.32$ ) in SBN53 ceramics when there is no liquid phase present in the matrix (for the T5-T15 samples). However, if template growth is assisted by a liquid in the matrix (i.e., for T5-15), a template concentration as low as 5 wt% is sufficient to attain an  $f = 0.98$  while keeping  $r = 0.29$ . A similar result was also observed in alumina textured by TGG.<sup>18</sup> Comparison of the T5 and T5-15 samples in Fig. 3 reveals that templates grow more in the T5-15 due to a liquid in the matrix, which results in faster consumption of the matrix grains.

## B. Dielectric properties

The phase transition becomes narrower with increasing sintering conditions for all compositions [see Fig. 5(a) for the T9 $\perp$  samples]. In other words,  $\gamma$  and  $C/K_{\text{max}}$  decrease with increasing  $f$  (Fig. 6). These results suggest that SBN53 compositions behave more like normal ferroelectrics (e.g.,  $\gamma$  is closer to 1), with relatively little dispersion with frequency. The higher  $C/K_{\text{max}}$  for samples with a lower  $f$  can be attributed to the inhomogeneous distribution of cations (e.g., more  $\text{K}^+$  and  $\text{Sr}^{2+}$  in the KSN templates and more  $\text{Ba}^{2+}$  in the matrix due to SN compensation<sup>3</sup>) between the elongated (e.g., textured) and matrix grains in the T5-T15 samples. At this stage, the compositional fluctuation from one grain to another can give rise to a range of Curie points, which broadens the phase transition.<sup>19,20</sup> The compositional fluctuations can be reduced with increasing sintering temperature or time. Therefore, the sharpening of the dielectric peak with increasing  $f$  may be attributed to the gradual homogenization of cations on the A sites. Note that the T5 samples still have weak relaxor behavior ( $T_{\text{max}}$  changes about 2 °C between 1 kHz and 100 kHz) even after sintering 1400 °C for 12 h presumably because of incomplete  $\text{K}^+$  homogenization between textured and matrix grains [Fig. 3(a)]. The T5-15 samples, however, have  $\gamma = 1.07$  and  $C/K_{\text{max}} = 25.9$  °C with no frequency dispersion, probably due to more uniform distribution of cations caused by liquid-phase sintering.

Increase in  $f$  resulted in enhanced dielectric properties. The highest  $K_{\text{max}}$  is obtained in the T9 $\perp$  samples ( $K_{\text{max}} = 23,600$ ) because the T9 samples attained a high  $f$  (0.93) and a low  $r$  value (0.32). However,  $K_{\text{max}} = 23,600$  is substantially less than the single-crystal values. For example,  $K_{\text{max}} = 81,000$ <sup>21</sup> and 40,000–63,000<sup>21,22</sup> were measured for SBN50 and SBN60

single crystals, respectively. The lower dielectric properties in textured samples can be attributed to the existence of nonferroelectric grain boundary phase(s). Excess  $\text{Nb}_2\text{O}_5$  contributed by the KSN templates forms a liquid during sintering and possibly forms a grain boundary phase(s) after cooling. This is more prevalent for the T5-15 samples because the excess  $\text{Nb}_2\text{O}_5$  is present both in the elongated grains and in the matrix, while excess  $\text{Nb}_2\text{O}_5$  is contained only in the elongated grains in the T5-T15 samples.<sup>3</sup> Therefore, the T5-15 samples probably have dielectrically thicker grain boundaries. Grain boundary phases considerably suppress the observed dielectric properties, especially at the  $T_{\text{max}}$ . Therefore, the T5-15 samples had a lower  $K_{\text{max}}$  (17,000) although they reached the highest  $f$  (0.98) and lowest  $r$  (0.29). SBN53 ceramics textured with a  $\text{V}_2\text{O}_5$  liquid former had much lower  $K_{\text{max}}$  (approximately 7,900).<sup>3</sup>

Another reason for the lower dielectric properties may be due to the presence of  $\text{K}^+$  ions. Analysis of dielectric properties in  $\geq 97\%$  dense random samples, with no abnormal grain growth, indicates that  $K_{\text{max}}$  decreases from 3520 for undoped samples to 2250 for 5 wt% and 1725 for 15.4 wt% KSN powder containing samples.  $K_{\text{max}}$  drops off very quickly when abnormal grain growth starts for each set. Similar results were observed in  $\text{K}^+$ ,  $\text{Li}^+$ , and  $\text{Na}^+$ -doped SBN ceramics.<sup>23</sup>

The increase in dielectric loss ( $\tan \delta$ ) in the  $c$  direction and decrease in the  $a$ - $b$  direction with increasing sintering time [Fig. 5(b)] can be attributed in part to the domain wall loss because the volume of the grains with uniform polarization increases with increasing  $f$ , which results in easier domain wall movement in the polar  $c$  direction. The evidence for this is that the dielectric loss of poled samples, measured as the temperature increased from 20 to 250 °C, was almost half of the dielectric loss of unpoled samples (e.g., 6.1% versus 12.3% at room temperature). The difference is probably attributable to a smaller number of domains and domain walls in the poled samples than the unpoled samples. Matrix grains that give isotropic properties are consumed by the template particles, and therefore, dielectric loss decreases in the nonpolar  $a$ - $b$  direction with increasing  $f$ .

$T_c$  mainly depends on the amount of KSN and the distribution of cations.  $T_c$  increases steadily after the completion of densification at 1300 °C, which may be due to (i) increase in  $f$  (and, thus, grain size) and (ii) diffusion of cations (primarily  $\text{K}^+$ ) into the SBN lattice, that is, compositional homogenization. A total of five out of six A sites are occupied by  $\text{Sr}^{2+}$  and  $\text{Ba}^{2+}$  ions; therefore, SBN is an empty bronze.<sup>24</sup> Alkali-metal elements, such as  $\text{Na}^+$  and  $\text{K}^+$  partially or fully occupy the interstitial vacant sites without vacancy formation,<sup>23,25,26</sup> which stabilizes the ferroelectric structure. Therefore,  $T_c$  increases due to the increased degree of filling of interstitial A sites with KSN content. Samples with  $\geq 9.1$  wt%

templates ( $f = 0.89$  to  $0.93$ ) have a  $T_c$  of  $124$ – $133$  °C compared to  $102$ – $108$  °C in the T5 samples ( $f = 0.61$ ) after sintering at  $1400$  °C for 12 h. The T5-15 samples had a  $T_c$  of  $150$ – $154$  °C, possibly due to more uniform cation distribution and, thus, more A site filling by the  $\text{K}^+$  ions. These results indicate that  $T_c$  in TGG samples is strongly correlated with  $f$  due to changes in KSN content. Pure SBN50 has a  $T_c$  between  $115$  and  $128$  °C, depending on the crystal quality.<sup>21,27–31</sup> This difference can be attributed to the different compositional variations and doping levels in the textured samples.

### C. Switching and piezoelectric properties

As is the case for the dielectric properties, the polarization is strongly enhanced in the  $c$  direction with increasing  $f$  (Fig. 9). The T5-15 $\perp$  samples reached a maximum  $P_r = 20.3$   $\mu\text{C}/\text{cm}^2$ . The estimated saturation polarization ( $P_{\text{sat}}$ ) from the  $P$ – $E$  loop is approximately  $24$   $\mu\text{C}/\text{cm}^2$  (“ $c_2$ ” in Fig. 8), which is  $69$ – $96\%$  of reported SBN50 single-crystal values. The average  $P_{\text{sat}}$  for single crystals is  $27.4$   $\mu\text{C}/\text{cm}^2$ , and it ranges from  $25$  to  $35$   $\mu\text{C}/\text{cm}^2$  depending on the quality of the grown crystal.<sup>31–33</sup> While  $P_r$  improves with  $f$  in the  $c$  direction, it decreases in the  $a$ – $b$  direction. For example, the T5// samples have a  $P_r = 1$   $\mu\text{C}/\text{cm}^2$  compared to  $0.5$   $\mu\text{C}/\text{cm}^2$  for the T5-15// samples after sintering at  $1400$  °C for 12 h. In addition,  $P_r$  (//-cuts) continuously decreases with increasing  $f$  due to the consumption of unoriented matrix grains because random samples have higher  $P_r$  than the //-cut samples due to averaging of properties (Fig. 8).

Figure 9 shows that the calculated maximum polarization from the model [Eq. (4)] is substantially higher than the measured data, particularly at lower  $f$  values. Possible reasons for lower  $P_r$  may be porosity, insulating  $\text{Nb}_2\text{O}_5$ -based grain boundary phase(s), pinning sites for domains within the elongated grains, poor continuity in the polarization, and randomly oriented matrix grains. Normalized  $P_r$  [i.e.,  $P_r(\text{calculated})/P_r(\text{measured})$ ] at  $f = 0.98$  indicates that a value as high as  $86\%$  of single crystal can be obtained by texturing.

Figure 9 further indicates that the  $P_r$  remains steady (and low) until nearly  $f \cong 0.5$  but increases considerably for higher  $f$ . The maximum polarization, obtained using Eq. (4) for a random sample, is half of the single crystal  $P_{\text{sat}}$  for  $180^\circ$  domain reversal. This was also theoretically calculated elsewhere.<sup>34</sup> Nevertheless, it is common for low-symmetry samples to display much lower remanent polarization values, as is the case here. This is believed to be because the random grains effectively decrease the measured polarization at lower  $f$  values, by preventing the charge transfer (to elongated grains) necessary for switching. That is, there are so few possible polarization directions that misoriented grains seriously degrade the ability to maintain continuity in the polarization vector during switching. As a result,

comparatively little of the material is actually able to switch. It is intriguing that the remanent polarization is virtually unchanged for  $f < 0.5$ . This suggests that for the cooperative switching process to occur effectively, it is necessary for well-oriented grains to have good connectivity. This would also account for the dramatic rise in the switchable polarization for  $f > 0.5$ . This requirement for percolation of well-oriented material should be less important in systems with more possible polarization directions (e.g., perovskites), since continuity of the polarization vector is much easier to achieve there. These results suggest that higher  $f$  and lower  $r$  are required to maximize the charge transfer to orient the domains and hence to increase the macroscopic polarization. Because the  $a$ – $b$  plane is nonpolar, higher  $r$  also degrades the percolation of the switchable grains.

The type of measurement, namely, type A and type B, also affects the properties in the  $c$  direction. Figure 7(a) shows several possible behaviors for  $P_r$  as a function of the amplitude of the field.  $P_r$  for T5 $\perp$  ( $f = 0.61$ ) increases with the field.  $P_r$  for T15 $\perp$  ( $f = 0.89$ ) decreases monotonically.  $P_r$  for T9 $\perp$  ( $f = 0.93$ ) shows an initial decrease followed by a shallow rise that was coupled with increased asymmetry in the  $P$ – $E$  loops. In type B measurements, however, no asymmetry was observed in any of the samples, and  $P_r$  was found to be higher [Fig. 7(b)]. The T5-15 samples reached the highest  $P_r$  in both measurements and did not experience fast polarization fatigue or asymmetric loops. The reason for higher  $P_r$  may be higher  $f$  and lower  $r$ , fewer grain boundaries, and more uniform cation distribution.

The above-mentioned results indicate that polarization fatigue becomes dominant with increasing  $f$  in the T5-T15 compositions. Polarization fatigue is defined as the gradual reduction of switchable charge with polarization reversal under bipolar drive. To further investigate the fatigue behavior in textured ceramics, the T15 $\perp$  sample sintered at  $1400$  °C for 12 h was subjected to a cycling experiment at  $50$  kV/cm,  $10$  Hz, and  $25$  °C.  $P_r$  decreased very fast from  $12.5$  to  $6.8$   $\mu\text{C}/\text{cm}^2$  after 10,000 cycles and gradually to  $5.4$   $\mu\text{C}/\text{cm}^2$  at 130,000 cycles.  $E_c$ , however, decreased slightly from  $7$  to  $6.2$  kV/cm after 130,000 cycles. No asymmetry was observed in the  $P$ – $E$  loops during cycling. Note that the T15 $\perp$  sample with  $\text{V}_2\text{O}_5$  liquid phase former did not experience polarization fatigue even after 130,000 cycles. Also, fatigue did not always increase with increasing  $P_r$ .

Fatigue is commonly observed in SBN single crystals. It was found in SBN50 that, after repeated switching under high fields, a major fraction of the total polarization rapidly locks into unswitching domain configurations after a few initial reversals. For example,  $P_{\text{sat}}$  drops from approximately  $28$   $\mu\text{C}/\text{cm}^2$  (1st cycle) to  $10$   $\mu\text{C}/\text{cm}^2$  (2nd cycle) and to  $6$   $\mu\text{C}/\text{cm}^2$  (3rd cycle) at  $60$  Hz and  $25$  °C.<sup>19</sup> A similar drastic decrease was also

observed in SBN75 single crystals.<sup>35</sup> Single crystals usually have imperfections such as striation bands (perpendicular to the  $c$  direction) that are mainly introduced during crystal growth, which results in a change in the stoichiometry.<sup>19,35</sup> Therefore, the switchable polarization could be clamped due to charges being stored at defects such as domain walls, dislocations, imperfections, and grain boundaries (for ceramics), which tends to break up the ferroelectric coupling. It was also observed that there was no asymmetry with respect to the electric field, indicating no net internal electric field, and therefore,  $E_c$  remained almost constant.<sup>35</sup>

The changes in polarization which occur on application of a cyclic field are principally due to the intrinsic (i.e., volume polarizability of the individual domains) and extrinsic (i.e., domain wall motion and reorientation effects) contributions.<sup>36</sup> There are at least two possible reasons for the effect of texture and processing on the observed fatigue behavior: changes in the sample homogeneity; changes in the character of the grain boundaries. As mentioned previously, SBN is an empty tungsten bronze in that 5  $\text{Sr}^{2+}$  or  $\text{Ba}^{2+}$  ions occupy the 6 available interstitial sites in the TTB structure. Therefore, high intrinsic channel defect concentrations due to vacant sites already exist in SBN. These channel defects are electrically neutral; however, short-range strain interactions may exist due to nonuniform distributions of  $\text{Ba}^{2+}$  and  $\text{Sr}^{2+}$  in the  $A_1$  and  $A_2$  sites, respectively.<sup>24</sup> For the T5-T15 samples,  $\text{K}^+$  ions may also contribute to this nonuniform cation and vacancy distribution. In addition, similar to the striation bands in the single crystals, the stoichiometry inside the elongated grains varies because

there are more  $\text{Sr}^{2+}$  and  $\text{K}^+$  ions in the center region (e.g., at the original KSN template position) and more  $\text{Ba}^{2+}$  ions in the grown region (due to excess BN in the matrix)<sup>3</sup>. Because  $\text{Ba}^{2+}$  and  $\text{K}^+$  ions diffuse slowly within the grains (e.g., by solid state diffusion), there may be an uneven distribution of cations and vacant sites, especially with increasing  $f$  or the size of elongated grains. Similar to charge trapping in the single crystals, compositional gradients within each grain could behave as defect sites for pinning the domains, which results in a decrease in  $P_r$  during polarization reversal. The fatigue rate intensifies with increasing  $f$  due to increased single-crystal regions (e.g., elongated grains) with more defect sites. For the T5-15 samples, however, lower polarization fatigue may be due to more uniform distribution of cations because these samples have  $\text{K}^+$  and  $\text{Nb}^{5+}$  ions both in the matrix and elongated grains, which results in less available pinning sites inside the elongated grains. A second possibility is that the differences in the fatigue behavior are due to differences in the electrical conductivity of the specimens due to changes in the grain boundary conductivity. In general, both T5-15 and samples containing  $\text{V}_2\text{O}_5$  specimens<sup>3</sup> had comparatively low dielectric loss values. These same samples had more marked suppression of the peak permittivities due to grain boundary phases. It is possible that lowered dielectric loss was partially associated with a change in the electrical conductivity and that resulting changes in charge injection also affected the fatigue rates.

Increased  $P_r$  after type B measurements in Fig. 7(b) suggest that fatigue is completely recoverable by annealing the samples above  $T_c$  (e.g., 500 °C for 1 h). These

TABLE II. The average room-temperature dielectric and piezoelectric properties for random and textured samples sintered at 1400 °C for 12 h.<sup>a</sup>

Sample	$T_c$ (°C) <sup>c</sup>	$K_{\max}$ <sup>d</sup>	$K$ at 25 °C <sup>d</sup>	$\tan \delta$ (%) <sup>e</sup>	$d_{33}$ (pC/N) <sup>f</sup>	$P_r$ ( $\mu\text{C}/\text{cm}^2$ ) <sup>g</sup>	$E_c$ (kV/cm) <sup>g</sup>
R0 <sup>b</sup>	129	2965	445	6.6	37	3.8	12.2
R5 <sup>b</sup>	138	2150	485	5.5	27	3.4	12.8
T5//	108	1065	610	1.9	1.4	1	8.5
T5⊥	102	9525	1485	7.7	27	6.7	5.9
R9 <sup>b</sup>	150	1525	290	3.8	26	2.7	15.8
T9//	124	860	520	1.1	0.9	0.8	11
T9⊥	126	21950	1325	10.1	61	12.9	6.9
R15 <sup>b</sup>	162	1055	300	2.1	30	1.5	13.9
T15//	133	865	480	1.2	1.1	0.9	13.2
T15⊥	128	18915	1325	10.3	52	11	6.9
T5-9//	144	570	325	0.6	1	0.3	5.9
T5-9⊥	144	16070	900	8.6	78	16.8	9.3
T5-15//	150	645	430	0.7	1.5	0.5	10.8
T5-15⊥	154	17000	935	7.4	83	20.3	10.6

<sup>a</sup>At least three measurements were averaged.

<sup>b</sup>Dielectric properties were measured at 100 kHz due to space charge effect.

<sup>c</sup> $T_c$ : temperature at the  $K_{\max}$  measured at 1 kHz during cooling.

<sup>d</sup> $K_{\max}$  and  $K$  at 25 °C: Measured at 1 kHz during cooling.

<sup>e</sup> $\tan \delta$  (%): Measured at room temperature and 1 kHz during cooling.

<sup>f</sup> $d_{33}$ : at 100 Hz and room temperature, after poling at 10 kV/cm at temperatures approximately 10–15 °C above  $T_c$ .

<sup>g</sup> $P_r$  and  $E_c$ : measured at room temperature and 10 Hz, for an applied field of 50 kV/cm (type B).

results indicate that domain wall pinning either by defect sites or by injected charge during polarization reversal is the main reason for the observed polarization fatigue in the highly textured SBN53 ceramics. Similar results were observed in  $\text{Pb}(\text{Zn}_{1/3}\text{Nb}_{2/3})\text{O}_3\text{-}4.5\text{PbTiO}_3$  single crystals.<sup>37</sup>

The best piezoelectric charge coefficient ( $d_{33}$ ) of 84 pC/N was obtained in the highly textured ( $f = 0.98$ ) T5-15± samples after sintering at 1400 °C for 12 h. This value is 76 to 93% of the SBN50 single crystals ( $d_{33} = 90$  to 110 pC/N for single crystals<sup>28,31,38–40</sup>). This sample also showed the highest  $P_r$ . For the T5-T15 samples, the maximum  $d_{33} = 63$  pC/N was measured in the T9± samples. This lower value can be attributed to inefficient poling. This is supported by the observation that  $P_r$  measured from a pyroelectric measurement is smaller than  $P_{\text{sat}}$  measured in  $P$ - $E$  loops. For example, the T15± sample sintered at 1400 °C for 4 h has a  $P_{\text{sat}}$  of 12.6  $\mu\text{C}/\text{cm}^2$  at room temperature obtained from a pyroelectric measurement (as the poled sample was heated from room temperature to 250 °C). However,  $P_{\text{sat}} = 17$   $\mu\text{C}/\text{cm}^2$  was estimated from the  $P$ - $E$  loop (type B) recorded at 50 kV/cm. This indicates inefficient domain orientation and, therefore, the  $d_{33}$  values are lower.

The pertinent average room-temperature dielectric, switching, and piezoelectric properties for random and textured samples sintered at 1400 °C for 12 h are summarized in Table II as a function of crystallographic direction and composition. Random samples have higher Curie temperatures compared to textured samples. The reasons could be more effective  $\text{K}^+$  homogenization in the random samples (i.e., fine KSN powder versus acicular template particles) and stress relief due to cracking.<sup>14</sup>

These results indicate that electrical properties are considerably improved, compared to randomly oriented samples, and highly anisotropic properties similar to single crystal values can be achieved in the samples textured by TGG.

## V. CONCLUSIONS

Highly textured (98%)  $\text{Sr}_{0.53}\text{Ba}_{0.47}\text{Nb}_2\text{O}_6$  ceramics were reactively sintered in a matrix of  $\text{SrNb}_2\text{O}_6$  and  $\text{BaNb}_2\text{O}_6$  powders. Acicular  $\text{KSr}_2\text{Nb}_5\text{O}_{15}$  particles were used to texture the samples in [001]. Samples had a phase-pure tetragonal tungsten bronze structure by 1200 °C and reached  $\geq 95\%$  of the theoretical density after sintering for 4 h at 1300 °C. The dielectric and piezoelectric properties were affected particularly by texture fraction ( $f$ ), degree of orientation parameter ( $r$ ), and grain boundary phases. Properties were enhanced in the samples with higher  $f$  and lower  $r$  values. In addition, the presence of nonferroelectric phases (mainly  $\text{Nb}_2\text{O}_5$ -based) at the grain boundaries suppressed the observed dielectric properties, especially at the  $T_c$ . For the samples with uniform cation distribution, dielectric spectra

showed normal ferroelectric behavior and fast polarization fatigue was not observed. The best electrical properties obtained are the peak dielectric constant of 23,600 (at  $T_c = 128$  °C), the remanent polarization ( $P_r$ ) of 20.3  $\mu\text{C}/\text{cm}^2$ , the estimated saturation polarization of 24  $\mu\text{C}/\text{cm}^2$  (69–96% of SBN50 single crystal), and the piezoelectric charge coefficient of 84 pC/N (76–93% of SBN50 single crystal). A model was developed to correlate processing parameters ( $f$  and  $r$ ) to the polarization.  $P_r$  increased sharply (i.e., after  $f \cong 0.5$ ) when the charge transfer (via percolation) between elongated grains was effectively established.

## ACKNOWLEDGMENTS

This work was supported by Office of Naval Research Grant N00014-98-1-0527. The authors also thank Huseyin Yilmaz and Edward Sabolsky for their helpful discussions at various stages of this work. C.D. gratefully acknowledges the support of the Gebze Institute of Technology (Gebze, Turkey) for his Ph.D. study in the United States.

## REFERENCES

1. K. Shoji and Y. Uehara, *Jpn. J. Appl. Phys.* **30**, 2315 (1991).
2. K. Nagata, Y. Yamamoto, H. Igarashi, and K. Okazaki, *Ferroelectrics* **38**, 853 (1981).
3. C. Duran, S. Trolier-McKinstry, and G.L. Messing, *J. Am. Ceram. Soc.* **83**, 2203 (2000).
4. C. Duran, G.L. Messing, and S. Trolier-McKinstry, *J. Cryst. Growth* (2002, submitted for publication).
5. M.M. Seabaugh, M.D. Vaudin, J.P. Cline, and G.L. Messing, *J. Am. Ceram. Soc.* **83**, 2049 (2000).
6. M.D. Vaudin, *TexturePlus* (National Institute of Standards and Technology, Ceramics Division, Gaithersburg, MD, 1999).
7. A. March, *Z. Kristallogr.* **81**, 285 (1932).
8. W.A. Dollase, *J. Appl. Crystallogr.* **19**, 267 (1986).
9. V.V. Kirillov and V.A. Isupov, *Ferroelectrics*, **5**, 3 (1973).
10. K. Uchino and S. Nomura, *Ferroelectr. Lett. Sect.* **44**, 55 (1982).
11. S.J. Butcher and N.W. Thomas, *J. Phys. Chem. Solids*, **52**, 595 (1991).
12. C.L. Choy, W.P. Leung, T.G. Xi, Y. Fei, and C.F. Shao, *J. Appl. Phys.* **71**, 170 (1992).
13. NIH Image, V.1.56, by W. Rasband, National Institutes of Health, Washington, DC.
14. C. Duran, G.L. Messing, and S. Trolier-McKinstry, *J. Mater. Sci.* (2002).
15. H-Y. Lee and R. Freer, *J. Appl. Phys.* **81**, 376 (1997).
16. H-Y. Lee and R. Freer, *J. Mater. Sci.* **33**, 1703 (1998).
17. J.R. Carruthers and M. Grasso, *J. Electrochem. Soc.: Solid State Sci.* **117**, 1426 (1970).
18. E. Suvaci and G.L. Messing, *J. Am. Ceram. Soc.* **83**, 2041 (2000).
19. T.W. Cline, Ph.D. Thesis, Pennsylvania State University (1977).
20. G.A. Smolenski and V.A. Isupov, *Zh. Tekh. Fiz.* **24**, 1375 (1954).
21. A.M. Glass, *J. Appl. Phys.* **40**, 4699 (1969).
22. R.R. Neurgaonkar, W.W. Ho, W.K. Cory, W.F. Hall, and L.E. Cross, *Ferroelectrics* **51**, 185 (1984).
23. A. Bhanumathi, S.N. Murty, K. Umakantham, K.C. Mouli, G. Padmavathi, K.T. Rao, and V. Syamalamba, *Ferroelectrics* **102**, 173 (1990).

24. D. Viehland, Z. Xu, and W-H. Huang, *Philos. Mag. A* **71**, 205 (1995).
25. S.N. Murty, K.V.R. Murty, K.C. Mouli, A. Bhanumathi, S.B. Raju, G. Padmavathi, and K.L. Murty, *Ferroelectrics* **158**, 325 (1994).
26. K. Umakantham, S.N. Murty, K.S. Rao, and A. Bhanumathi, *J. Mater. Sci. Lett.* **6**, 565 (1987).
27. R.R. Neurgaonkar, W.K. Cory, J.R. Oliver, E.J. Sharp, G.L. Wood, and G.J. Salamo, *Ferroelectrics* **142**, 167 (1993).
28. R.R. Neurgaonkar, W.K. Cory, and J.R. Oliver, *Ferroelectrics* **51**, 3 (1983).
29. R. Guo, A.S. Bhalla, G. Burns, and F.H. Dacol, *Ferroelectrics* **93**, 397 (1989).
30. M. DiDomenico, Jr. and S.H. Wemple, *J. Appl. Phys.* **40**, 720 (1969).
31. R.R. Neurgaonkar, W.F. Hall, J.R. Oliver, W.W. Ho, and W.K. Cory, *Ferroelectrics* **87**, 167 (1988).
32. S.B. Deshpande, H.S. Potdar, P.D. Godbole, and S.K. Date, *J. Am. Ceram. Soc.* **75**, 2581 (1992).
33. I. Camlibel, *J. Appl. Phys.* **40**, 1690 (1969).
34. T. Takenaka and K. Sakata, *Jpn. J. Appl. Phys.* **19**, 31 (1980).
35. B. Jimenez, C. Alemany, J. Mendiola, and E. Maurer, *Ferroelectrics* **38**, 841 (1981).
36. D.A. Payne, Ph.D. Thesis, Pennsylvania State University (1973).
37. K. Takemura, M. Ozgul, V. Bornand, S. Trolier-McKinstry, and C.A. Randall, *J. Appl. Phys.* **88**, 7272 (2000).
38. R.R. Neurgaonkar, J.R. Oliver, W.K. Cory, L.E. Cross, and D. Viehland, *Ferroelectrics* **160**, 265 (1994).
39. S.T. Liu, *Ferroelectrics* **22**, 709 (1978).
40. T.W. Cline, L.E. Cross, and S.T. Liu, *J. Appl. Phys.* **49**, 4298 (1978).